Journal of Sound and Vibration (1999) **225**(1), 127–152
Article No. jsvi.1999.2230, available online at http://www.idealibrary.com on IDEAL®

MULTI-MODAL GEOMETRICAL NON-LINEAR FREE VIBRATION OF FULLY CLAMPED COMPOSITE LAMINATED PLATES

P. RIBEIRO

DEMEGI, Faculdade de Engenharia, Universidade do Porto, Rua dos Bragas, 4099 Porto Codex, Portugal

AND

M. PETYT

Institute of Sound and Vibration Research, Univerity of Southampton, Southampton SO17 1BJ, U.K.

(*Received* 6 *August* 1998, *and in final form* 23 *February* 1999)

The geometrically non-linear free vibration of thin composite laminated plates is investigated using the hierarchical finite-element (HFEM) and the harmonic-balance methods (HBM). Von Kármán's non-linear strain–displacement relationships are employed and the mid-plane in-plane displacements are included in the model. The equations of motion are developed by applying the principle of virtual work and are solved by a continuation method. The convergence properties of the HFEM and of the HBM are analyzed. Internal resonances are discovered and the consequent multi-modal and multi-frequency vibration of the plates is shown. The variation of the plates' mode shape and the effect of the fibres' orientation are investigated.

1. INTRODUCTION

Due to their high stiffness to weight ratio, laminated composite plates are used in commercial and military aircraft [1], where they are often subjected to high levels of acoustic pressure. Therefore, they may vibrate with large amplitude displacements, i.e., with geometrical non-linearity.

The resonance frequencies of a plate change with the amplitude of vibration displacement [2–7], possibly becoming commensurable with other resonance frequencies and causing coupling of the natural modes. As a result, energy is interchanged between those modes and the response is multi-modal. This phenomenon is known as internal resonance [8–10].

Lau *et al.* [11] used the finite-element method and the harmonic-balance method to study the vibration of isotropic plates. The curves were traced by incrementing selectively the fastest varying characteristic amplitude or the frequency. Loops due to 1 : 3 internal resonances were found. Abe *et al.* [12] analyzed internal resonances

0022-460X/99/310127 + 26 $30.00/0

in laminated plates subjected to harmonic excitations by applying the Galerkin procedure and the perturbation method of multiple scales. The method is only valid for displacements smaller than the thickness of the plate. The in-plane displacements were neglected and the transverse deflection was assumed to be a function of two linear, thus constant, modes.

The study of the free vibrations of undamped non-linear systems, namely the determination of the amplitude–frequency relations and modes of vibration, is important because the dynamic properties of the system are estimated. It is known that the non-linear mode shapes [13] of plates with fixed ends change with amplitude [2–6]. This variation can be described by a finite-element method (FEM) model. The motion of plates vibrating freely with amplitude displacements of the order of their thickness is generally periodic [14] and, consequently, can be analyzed by the harmonic-balance method (HBM) [8, 15, 16]. Unlike perturbation methods, the HBM is not restricted to weakly non-linear problems.

Generally, the solution of the non-linear equations of motion can only be obtained approximately and iteratively, with a recalculation of the non-linear stiffness matrix in each iteration. Thus, the time needed to obtain the solutions increases considerably with the number of degrees of freedom (d.o.f.). The internal resonance phenomenon results in a significant excitation of higher order modes, which require a spatial model with more degrees of freedom for accuracy. Moreover, to study multi-frequency vibrations by the HBM more than one harmonic is needed in the time series, consequently increasing the total number of d.o.f. and, in general, a problem involving a composite plate is not symmetric, thus precluding a reduction of the number of d.o.f. using symmetries of the system.

In the hierarchical finite-element method (HFEM), better approximations are accomplished by adding higher order shape functions to the existing model, without redefining the mesh. Because convergence tends to be achieved with a small number of d.o.f. [4–7], this method is very suitable for non-linear analyses.

In this paper, the HFEM and HBM are used to analyze the free vibration with large displacements of thin, rectangular, composite laminated, fully clamped plates. The convergence with the number of harmonics and with the number of shape functions is discussed. Internal resonances are detected and the effect they have on the dynamic behaviour of the laminated plates is described.

2. MATHEMATICAL MODEL

2.1. HIERARCHICAL FINITE-ELEMENT METHOD

For each element, the mid-plane displacements (Figure 1) are expressed in the form

$$\begin{Bmatrix} u_0 \\ v_0 \\ w_0 \end{Bmatrix} = [\mathbf{N}] \begin{Bmatrix} \mathbf{q}_p \\ \mathbf{q}_w \end{Bmatrix}, \tag{1}$$

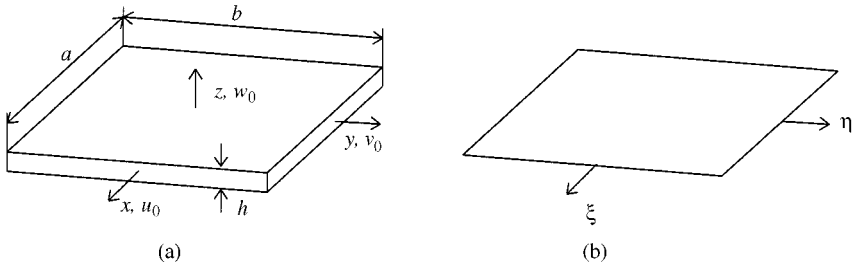

Figure 1. (a) Rectangular plate: x, y and z—global co-ordinate system; u_0, v_0 and w_0—mid-plane displacements; a, b and h—plate dimensions, (b) ξ, η—local co-ordinate system.

$$[\mathbf{N}] = \begin{bmatrix} \lfloor \mathbf{N}^u \rfloor & 0 & 0 \\ 0 & \lfloor \mathbf{N}^u \rfloor & 0 \\ 0 & 0 & \lfloor \mathbf{N}^w \rfloor \end{bmatrix}, \tag{2}$$

$$\lfloor \mathbf{N}^u \rfloor = \lfloor\, g_1(\xi)g_1(\eta)g_1(\xi)g_2(\eta) \cdots g_{p_i}(\xi)g_{p_i}(\eta) \,\rfloor, \tag{3}$$

$$\lfloor \mathbf{N}^w \rfloor = \lfloor\, f_1(\xi)f_1(\eta)f_1(\xi)f_2(\eta) \cdots f_{p_o}(\xi)f_{p_o}(\eta) \,\rfloor, \tag{4}$$

where p_o and p_i are the number of out-of-plane and in-plane shape functions used in the model, $\{\mathbf{g}\}$ and $\{\mathbf{f}\}$ are vectors of in- and out-of-plane shape functions, $\{\mathbf{q}_p\}$ and $\{\mathbf{q}_w\}$ are the generalized in- and out-of-plane displacements and $[\mathbf{N}]$ is the matrix of shape functions. The set of shape functions used is the Rodrigues' form of Legendre polynomials [4, 7, 14].

For smooth solutions, p-extensions are more advantageous than strong mesh generations [17]. Consequently, only one element is used to model the whole plate (for irregular geometries more elements can be used), and the local and global co-ordinates, Figure 1, are related by

$$\xi = 2x/a, \qquad \eta = 2y/b. \tag{5}$$

Von Kármán's non-linear strain–displacement relationships are valid for thin plates [18]. They can be expressed as

$$\begin{Bmatrix} \varepsilon_x \\ \varepsilon_y \\ \gamma_{xy} \end{Bmatrix} = \begin{bmatrix} 1 & 0 & 0 & z & 0 & 0 \\ 0 & 1 & 0 & 0 & z & 0 \\ 0 & 0 & 1 & 0 & 0 & z \end{bmatrix} \{\boldsymbol{\varepsilon}\} = [[\mathbf{I}]\, z[\mathbf{I}]]\{\boldsymbol{\varepsilon}\}, \tag{6}$$

where

$$\{\boldsymbol{\varepsilon}\} = \begin{Bmatrix} \boldsymbol{\varepsilon}_o^p \\ \boldsymbol{\varepsilon}_o^b \end{Bmatrix} + \begin{Bmatrix} \boldsymbol{\varepsilon}_L^p \\ 0 \end{Bmatrix}, \tag{7}$$

$\{\boldsymbol{\varepsilon}_0^p\}$ and $\{\boldsymbol{\varepsilon}_0^b\}$ are the linear membrane and bending strains, and $\{\boldsymbol{\varepsilon}_L^p\}$ is the geometrically non-linear membrane strain. These strains are defined as

$$\{\boldsymbol{\varepsilon}_o^p\} = \begin{Bmatrix} u_{,x} \\ v_{,y} \\ u_{,y} + v_{,x} \end{Bmatrix}, \qquad \{\boldsymbol{\varepsilon}_o^b\} = \begin{Bmatrix} -w_{,xx} \\ -w_{,yy} \\ -2w_{,xy} \end{Bmatrix}, \qquad \{\boldsymbol{\varepsilon}_L^p\} = \begin{Bmatrix} (w_{,x})^2/2 \\ (w_{,y})^2/2 \\ w_{,x}w_{,y} \end{Bmatrix}, \tag{8}$$

where $,x$ represents differentiation with respect to x.

In the absence of external forces, the equations of motion are derived by equating the sum of the virtual work of the inertia forces and of the elastic restoring forces to zero. Neglecting rotatory inertia—it can be neglected for most engineering applications of thin plates [18]—and using the constitutive relations of the plate [18] one obtains

$$\int_\Omega (\{\delta\boldsymbol{\varepsilon}_o^p\}^{\mathrm{T}} + \{\delta\boldsymbol{\varepsilon}_L^p\}^{\mathrm{T}})[\mathbf{A}](\{\boldsymbol{\varepsilon}_o^p\} + \{\boldsymbol{\varepsilon}_L^p\})\,\mathrm{d}\Omega + \int_\Omega \{\delta\boldsymbol{\varepsilon}_o^b\}^{\mathrm{T}}[\mathbf{D}]\{\boldsymbol{\varepsilon}_o^b\}\,\mathrm{d}\Omega$$

$$+ \int_\Omega \rho h(\delta u_0\ddot{u}_0 + \delta v_0\ddot{v}_0 + \delta w_0\ddot{w}_0)\,\mathrm{d}\Omega = 0, \tag{9}$$

where ρ denotes the mass per unit volume and Ω the area of the plate. $[\mathbf{A}]$ and $[\mathbf{D}]$ are the membrane and flexural rigidity matrices given by

$$(A_{ij}, D_{ij}) = \sum_{k=1}^{NL} \int_{z_{k-1}}^{z_k} (1, z^2) C_{ij}^{(k)} \mathrm{d}z, \quad i, j = 1, 2 \text{ and } 6, \tag{10}$$

where $C_{ij}^{(k)}$ are the reduced stiffnesses of the kth layer, which can be obtained from E_L, E_T, major and minor Young's moduli, from the Poisson ratios v_{LT} and v_{TL} and from the shear modulus G_{LT} [18]. The indices i and j assume the value 1, 2 and 6, because the terms $C_{ij}^{(k)}$ result from a simplification of the generalized Hooke's law, which is expressed by means of a (6×6) matrix. L and T denote the principal directions of the orthotropic plate layer. ρ denotes the mass per unit volume and Ω the area of the plate. Only symmetric laminated plates will be analyzed, consequently, there is no coupling between in-plane stretching and transverse bending.

Substituting equations (8) into equation (9), allowing the virtual generalized displacements to be arbitrary, neglecting in-plane inertia and eliminating the generalized in-plane co-ordinates $\{\mathbf{q}_p\}$, results in the following equations of motion:

$$[\mathbf{M}_b]\{\ddot{\mathbf{q}}_w\} + [\mathbf{K}_{1b}]\{\mathbf{q}_w\} + [\mathbf{K}nl]\{\mathbf{q}_w\} = \{\mathbf{0}\}, \tag{11}$$

where the non-linear stiffness matrix, which is a quadratic function of the generalized transverse displacements $\{\mathbf{q}_w\}$, is defined as

$$[\mathbf{K}nl] = [\mathbf{K}_4] - 2[\mathbf{K}_2]^{\mathrm{T}}[\mathbf{K}_{1p}]^{-1}[\mathbf{K}_2]. \tag{12}$$

$[\mathbf{M}_b]$ is the bending inertia matrix; $[\mathbf{K}_{1p}]$ and $[\mathbf{K}_{1b}]$ are the in-plane and bending linear stiffness matrices; $[\mathbf{K}_2]$ and $[\mathbf{K}_4]$ are the non-linear stiffness matrices. These matrices are defined in references [4, 14]. The system of equations (11) constitutes a system of coupled Duffing equations.

2.2. HARMONIC BALANCE METHOD

Experimental, analytical and numerical investigations demonstrate that periodic motions are the most likely to occur in plates vibrating freely with amplitudes of the order of their thickness [14]. In this paper, undamped periodic motions will be analyzed and, consequently, the transverse generalized displacement may be expressed as

$$\{\mathbf{q}_w\} = \sum_{i=1,3}^{2k=1} \{\mathbf{w}_i\} \cos(i\omega t). \tag{13}$$

Inserting equations (13) into the equations of motion (11) and implementing the HBM, the equations of motion in the frequency domain are derived. These are of the form

$$\{\mathbf{F}(\{\mathbf{w}\}, \omega^2)\} = (-\omega^2[\mathbf{M}] + [\mathbf{KL}] + [\mathbf{KNL}(\{\mathbf{w}\})])\{\mathbf{w}\} = \{\mathbf{0}\}, \tag{14}$$

where $[\mathbf{M}]$ represents the mass matrix, $[\mathbf{KL}]$ the linear stiffness matrix and $[\mathbf{KNL}(\{\mathbf{w}\})]$ the non-linear stiffness matrix, which depends quadratically on the generalized displacements $\{\mathbf{w}\}$. The total number of degrees of freedom of the model is $n = kp_o^2$, where k is the number of terms considered in equation (13). All integrals involved in calculating the inertia and stiffness matrices were evaluated using symbolic computation [19].

One, two and three harmonics will be used in the numerical applications and the equations of motion are derived for the last, more general, case. When $k = 3$ in equation (13), the vector of transverse generalized displacements is given by

$$[\mathbf{q}_w(t)\} = \{\mathbf{w}_1\} \cos(\omega t) + \{\mathbf{w}_3\} \cos(3\omega t) + \{\mathbf{w}_5\} \cos(5\omega t). \tag{15}$$

Substituting expressions (15) into the equations of motion (14) and neglecting harmonics higher than $5\omega t$, the following equations of motion are obtained:

$$\left(-\omega^2 \begin{bmatrix} [\mathbf{M}_b] & 0 & 0 \\ 0 & 9[\mathbf{M}_b] & 0 \\ 0 & 0 & 25[\mathbf{M}_b] \end{bmatrix} + \begin{bmatrix} [\mathbf{K}_{1b}] & 0 & 0 \\ 0 & [\mathbf{K}_{1b}] & 0 \\ 0 & 0 & [\mathbf{K}_{1b}] \end{bmatrix} \right) \begin{Bmatrix} \mathbf{w}_1 \\ \mathbf{w}_3 \\ \mathbf{w}_5 \end{Bmatrix} + \begin{Bmatrix} \mathbf{F}_{c1} \\ \mathbf{F}_{c3} \\ \mathbf{F}_{c5} \end{Bmatrix} = \begin{Bmatrix} 0 \\ 0 \end{Bmatrix}, \tag{16}$$

where, comparing with equation (14), the first matrix is the mass matrix $[\mathbf{M}]$ and the second is the linear stiffness matrix $[\mathbf{KL}]$. The new vector of generalized

displacements, $\{\mathbf{w}\}$, does not depend on time and is defined as

$$\{\mathbf{w}\} = \begin{Bmatrix} \mathbf{w}_1 \\ \mathbf{w}_3 \\ \mathbf{w}_5 \end{Bmatrix}. \tag{17}$$

The cubic non-linear terms—$\{\mathbf{F}_{c1}\}$, $\{\mathbf{F}_{c3}\}$ and $\{\mathbf{F}_{c5}\}$—are defined by

$$\{\mathbf{F}_{c1}\} = \frac{2}{T}\int_0^T [\mathbf{K}nl]\{\mathbf{q}_w\}\cos(\omega t)\,\mathrm{d}t, \tag{18}$$

$$\{\mathbf{F}_{c2}\} = \frac{2}{T}\int_0^T [\mathbf{K}nl]\{\mathbf{q}_w\}\cos(3\omega t)\,\mathrm{d}t, \tag{19}$$

$$\{\mathbf{F}_{c3}\} = \frac{2}{T}\int_0^T [\mathbf{K}nl]\{\mathbf{q}_w\}\cos(5\omega t)\,\mathrm{d}t \tag{20}$$

and are given by

$$\begin{Bmatrix} \mathbf{F}_{c1} \\ \mathbf{F}_{c3} \\ \mathbf{F}_{c5} \end{Bmatrix} = [\mathbf{KNL}] \begin{Bmatrix} \mathbf{w}_1 \\ \mathbf{w}_3 \\ \mathbf{w}_5 \end{Bmatrix}. \tag{21}$$

The non-linear stiffness matrix, $[\mathbf{KNL}]$, is

$$[\mathbf{KNL}] = \frac{1}{4}\left(\begin{bmatrix} 3[\mathbf{KNL}_1] & [\mathbf{KNL}_1] & \mathbf{0} \\ [\mathbf{KNL}_1] & 2[\mathbf{KNL}_1] & [\mathbf{KNL}_1] \\ \mathbf{0} & [\mathbf{KNL}_1] & 2[\mathbf{KNL}_1] \end{bmatrix}\right.$$

$$+ 2\begin{bmatrix} [\mathbf{KNL}_2] & 2[\mathbf{KNL}_2] & [\mathbf{KNL}_2] \\ 2[\mathbf{KNL}_2] & \mathbf{0} & [\mathbf{KNL}_2] \\ [\mathbf{KNL}_2] & [\mathbf{KNL}_2] & \mathbf{0} \end{bmatrix}$$

$$\left. + 2\begin{bmatrix} \mathbf{0} & [\mathbf{KNL}_3] & 2[\mathbf{KNL}_3] \\ [\mathbf{KNL}_3] & [\mathbf{KNL}_3] & \mathbf{0} \\ 2[\mathbf{KNL}_3] & \mathbf{0} & \mathbf{0} \end{bmatrix} + \begin{bmatrix} 2[\mathbf{KNL}_4] & \mathbf{0} & [\mathbf{KNL}_4] \\ \mathbf{0} & 3[\mathbf{KNL}_4] & \mathbf{0} \\ [\mathbf{KNL}_4] & \mathbf{0} & 2[\mathbf{KNL}_4] \end{bmatrix}\right)$$

$$+2\begin{bmatrix}[\mathbf{KNL}_5] & [\mathbf{KNL}_5] & \mathbf{0}\\ [\mathbf{KNL}_5] & \mathbf{0} & 2[\mathbf{KNL}_5]\\ \mathbf{0} & 2[\mathbf{KNL}_5] & \mathbf{0}\end{bmatrix}+\begin{bmatrix}2[\mathbf{KNL}_6] & \mathbf{0} & \mathbf{0}\\ \mathbf{0} & 2[\mathbf{KNL}_6] & \mathbf{0}\\ \mathbf{0} & \mathbf{0} & 3[\mathbf{KNL}_6]\end{bmatrix}\Bigg). \tag{22}$$

$[\mathbf{KNL}_i]$ are of the form

$$[\mathbf{KNL}_i(\{\mathbf{w}_c\},\{\mathbf{w}_c^*\})]=[\mathbf{K}_4(\{\mathbf{w}_c\},\{\mathbf{w}_c^*\})]-[\mathbf{K}_2(\{\mathbf{w}_c\})]^{\mathrm{T}}[\mathbf{K}_{1p}]^{-1}[\mathbf{K}_2(\{\mathbf{w}_c^*\})]$$

$$-[\mathbf{K}_2(\{\mathbf{w}_c^*\})]^{\mathrm{T}}[\mathbf{K}_{1p}]^{-1}[\mathbf{K}_2(\{\mathbf{w}_c\rangle)], \tag{23}$$

where $[\mathbf{K}_4(\{\mathbf{w}_c\},\{\mathbf{w}_c^*\})]$ means that matrix $[\mathbf{K}_4]$ is a quadratic function of $\{\mathbf{w}_c\}$ and $\{\mathbf{w}_c^*\}$. $\{\mathbf{w}_c\}=\{\mathbf{w}_c^*\}=\{\mathbf{w}_1\}$ for $[\mathbf{KNL}_1]$, $\{\mathbf{w}_c\}=\{\mathbf{w}_1\}$, $\{\mathbf{w}_c^*\}=\{\mathbf{w}_3\}$ for $[\mathbf{KNL}_2]$, $\{\mathbf{w}_c\}=\{\mathbf{w}_1\}$, $\{\mathbf{w}_c^*\}=\{\mathbf{w}_5\}$ for $[\mathbf{KNL}_3]$, $\{\mathbf{w}_c\}=\{\mathbf{w}_c^*\}=\{\mathbf{w}_3\}$ for $[\mathbf{KNL}_4]$, $\{\mathbf{w}_c\}=\{\mathbf{w}_3\}$, $\{\mathbf{w}_c^*\}=\{\mathbf{w}_5\}$ for $[\mathbf{KNL}_5]$ and $\{\mathbf{w}_c\}=\{\mathbf{w}_c^*\}=\{\mathbf{w}_5\}$ for $[\mathbf{KNL}_6]$.

3. THE CONTINUATION METHOD

3.1. PREDICTOR–CORRECTOR PROCEDURE

The equations of motion (14) are solved by a continuation method [20, 21], which is composed of two main loops. In the external loop a prediction to the solution is defined using the two last determined points of the backbone curve (curve that relates the frequency with the amplitude of vibration)—$(\{\mathbf{w}\}_i, \omega_i^2)$ and $(\{\mathbf{w}\}_{i-1}, \omega_{i-1}^2)$. The prediction of $\{\mathbf{w}\}_{i+1}$ is thus obtained in the following way:

$$\{\mathbf{w}\}_{i+1}=\{\mathbf{w}\}_i+\Delta\{\mathbf{w}\}_{i+1},\qquad \Delta\{\mathbf{w}\}_{i+1}=(\{\mathbf{w}\}_i-\{\mathbf{w}\}_{i-1})\frac{\mathrm{d}w\,aux}{\Delta w}, \tag{24}$$

where dw *aux* is the amplitude of the first increment vector, $\Delta\{\mathbf{w}\}_{i+1}$ and Δw is the amplitude of the vector $(\{\mathbf{w}\}_i-\{\mathbf{w}\}_{i-1})$. The subscript i represents iterations of the external loop, and the different points of the curve; the subscript *previous* represents a former solution of the internal loop, which is discarded. A prediction for ω_{i+1}^2 must also be calculated. This results from the equation

$$\omega_{i+1}^2=\omega_i^2+\Delta\omega_0^2,\qquad \Delta\omega_0^2=\pm\, s/(\{s\mathbf{w}\}_1^{\mathrm{T}}\{s\mathbf{w}\}_1)^{1/2}, \tag{25}$$

where s and $\{\delta\mathbf{w}\}_1$ will be defined later. The sign of $\Delta\omega_0^2$ is the same as the one of the previous increment, unless the determinant of the Jacobian of $\{\mathbf{F}\}$ has changed sign, in which case a sign reversal is applied. The Jacobian of $\{\mathbf{F}\}$, $[\mathbf{J}]$, is defined by

$$[\mathbf{J}]=\partial\{\mathbf{F}\}/\partial\{\mathbf{w}\}. \tag{26}$$

The correction of the approximated solution is carried out in an internal loop. Applying Newton's method to equation (14) and considering also variations in the frequency of vibration, one obtains

$$[\mathbf{J}]\{\delta\mathbf{w}\} - [\mathbf{M}]\{\mathbf{w}\}_{i+1}\delta\omega^2 = -\{\mathbf{F}\}. \tag{27}$$

Because the frequency of vibration is unknown, another equation is needed. This is obtained by constraining the distance between the two successive points of the curve, the arc-length s, to a fixed value, by the following constraint equation:

$$s^2 = \| \Delta\{\mathbf{w}\}_{i+1} \|^2. \tag{28}$$

From equation (27),

$$\{\delta\mathbf{w}\} = \delta\omega^2\{\delta\mathbf{w}\}_1 + \{\delta\mathbf{w}\}_2, \qquad [\mathbf{J}]\{\delta\mathbf{w}\}_1 = [\mathbf{M}]\{\mathbf{w}\}_{i+1}, \qquad [\mathbf{J}]\{\delta\mathbf{w}\}_2 = -\{\mathbf{F}\}. \tag{29}$$

Then the corrected value of $\{\mathbf{w}\}$ is

$$\{\mathbf{w}\}_{i+1} = \{\mathbf{w}\}_i + \Delta\{\mathbf{w}\}_{i+1}, \qquad \Delta\{\mathbf{w}\}_{i+1} = (\Delta\{\mathbf{w}\}_{i+1})_{previous} + \{\delta\mathbf{w}\}. \tag{30}$$

Substituting $\Delta\{\mathbf{w}\}_{i+1}$ into constraint equation (28) gives the relation for $\delta\omega^2$. The corrected value of the natural frequency is given by

$$\omega_{i+1}^2 = \omega_i^2 + \Delta\omega_{i+1}^2, \qquad \Delta\omega_{i+1}^2 = (\Delta\omega_{i+1}^2)_{previous} + \delta\omega^2. \tag{31}$$

The iterations are repeated until the following inequalities:

$$\left|\frac{\delta\omega^2}{\omega_{i+1}^2}\right| < e_1, \qquad \frac{\| \{\delta\mathbf{w}\} \|}{\| \{\mathbf{w}\}_{i+1} \|} < e_2, \qquad \| \{\mathbf{F}\} \| < e_3 \tag{32}$$

are satisfied ($|\ |$ represents the absolute value and $\|\ \|$ the Euclidean norm, although other norms can be used). e_1, e_2 and e_3 assume values between 10^{-3} and 10^{-6}.

3.2. BIFURCATION POINTS AND BRANCH SWITCHING

An element $(\{\mathbf{w}\}_0, \omega_0^2)$ of a branch of solutions of $\{\mathbf{F}(\{\mathbf{w}\}, \omega^2)\} = \{\mathbf{0}\}$ is called an exceptional point—bifurcation or turning point—if the Jacobian of $\{\mathbf{F}\}$ with respect to $\{\mathbf{w}\}$ is singular [21]. In order to detect exceptional points, the sign of the determinant of $[\mathbf{J}]$ is studied for each new point of the backbone curve. If the signs of $|\mathbf{J}|$ of two successive points of the backbone curve are different, then there exists a particular point between those two points for which $|\mathbf{J}| = 0$ and the matrix $[\mathbf{J}]$ is singular. From bifurcation points, secondary branches are born.

In order to describe secondary branches, a point close to the bifurcation point is used to calculate the Jacobian matrix and the eigenvalue problem

$$([\mathbf{J}] - \mu[\mathbf{I}])\{\boldsymbol{\phi}\} = \{\mathbf{0}\} \tag{33}$$

is solved. The eigenvector(s) $\{\boldsymbol{\phi}\}_j$ associated with the zero eigenvalue(s) $\mu_j = 0$ indicate the direction(s) to be followed. The perturbed configuration, $\{\mathbf{w}\}_j$, that is used as the starting vector for branch switching [20, 21], is obtained by adding the scaled eigenvector to the solution vector $\{\mathbf{w}\}$ at the bifurcation point

$$\{\mathbf{w}\}_j = \{\mathbf{w}\} + \zeta_j \frac{\{\boldsymbol{\phi}\}_j}{\|\{\boldsymbol{\phi}\}_j\|}, \tag{34}$$

where ζ_j denotes a scaling factor whose value is defined by the user, in a "trial-and-error" way, until convergence to a solution in the new branch is achieved.

4. APPLICATIONS

4.1. INTRODUCTION

Two graphite/epoxy rectangular plates are analyzed. Their geometrical and material properties are defined in Tables 1 and 2. Plate 1 is a specially orthotropic laminated plate, which means that its bending and twisting stiffnesses are uncoupled. Also, as in symmetric laminates, the in-plane and bending stiffnesses are uncoupled [18]. Plate 2 is a symmetrically laminated plate. In order to analyze the

TABLE 1
Geometric properties of the plates

Plate	Number of layers	Orientation of principal axes	a (mm)	b (mm)	h (mm)
1	16	$(45, -45, 0, -45, 45, -45, 0, 45)_{\text{sym}}$	300	150	2·72
2	5	$(\theta, -\theta, \theta, -\theta, \theta)$	300	300	1

TABLE 2
Material properties of the plates

Plate	E_L (GN/m^2)	E_G (GN/m^2)	G_{LT} (GN/m^2)	ν_{LT}	ρ (Kg/m^3)
1	173·0	7·2	3·76	0·29	1540
2	173·0	E_L/15·4	0·79 E_G	0·3	1540

influence of the fibres orientation, two different values will be considered for the angle that defines the orientation of the fibres with respect to the x-axis in Plate 2: $\theta = 15$ and 45°. The plate's linear mode shapes and natural frequencies are shown in Figures 2–4.

In order to demonstrate that an accurate model can be constructed with a small number of degrees of freedom, the convergence with the number of harmonics and with the number of shape functions is discussed in Sections 4.2 and 4.3. Plates 1 and 2 with $\theta = 45^\circ$, referred to as Plate 2, are analyzed in these sections. Subsequently, in Section 4.4, internal resonances are detected and the effect they have on the dynamic behaviour of the plates is described. Finally, the influence of the fibre orientation is discussed.

4.2. CONVERGENCE WITH THE NUMBER OF HARMONICS

Figures 5 and 6 present the backbone curves of Plates 1 and 2 calculated with a different number of harmonics. w_m represents the maximum amplitude of vibration displacement attained during the cycle at the points (ξ, η) indicated and is given by

$$w_m = \lfloor \mathbf{N}_w \rfloor \sum_{i=1,3}^{2k-1} \{\mathbf{w}_i\}, \tag{35}$$

wehere k represents the number of harmonics. Two harmonics give accurate results and will be used in the models of both plates.

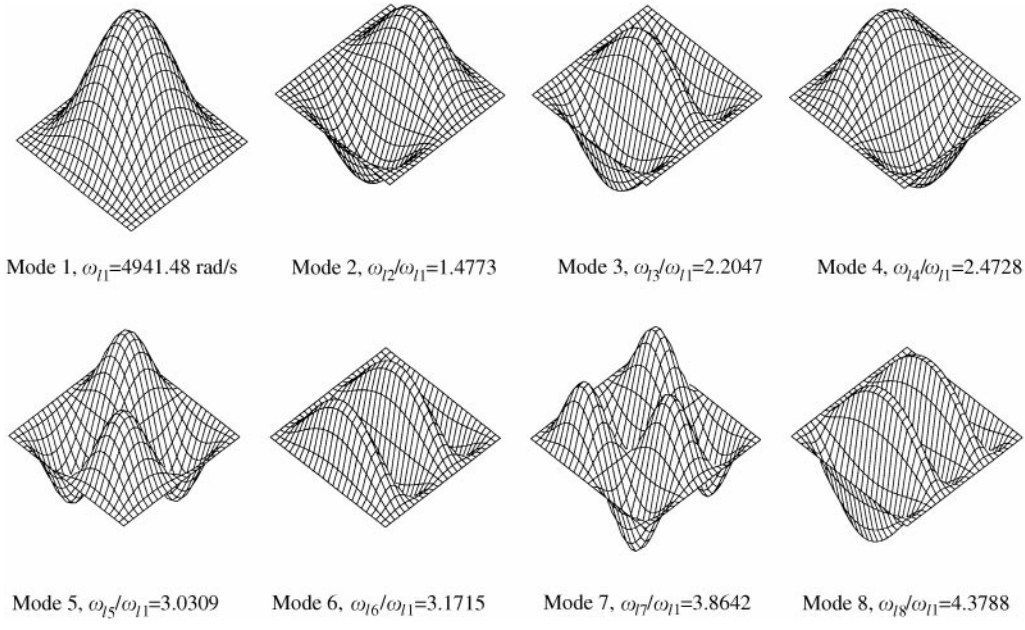

Figure 2. Linear mode shapes and natural frequencies of Plate 1. $p_o = 10$.

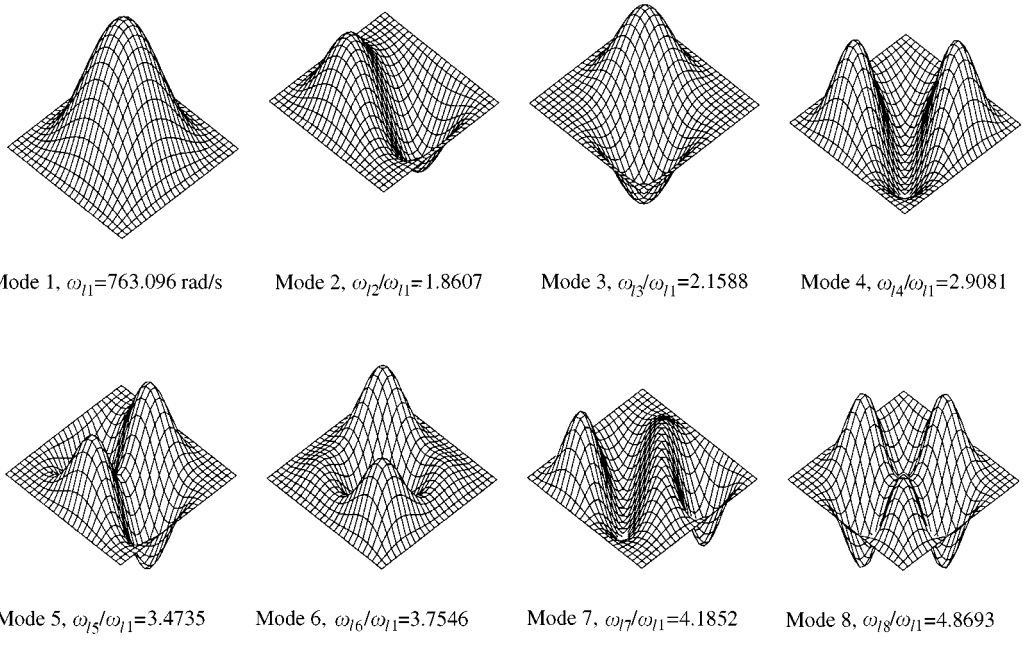

Figure 3. Linear mode shapes and natural frequencies of Plate 2, $\theta = 45^\circ$, $p_o = 8$.

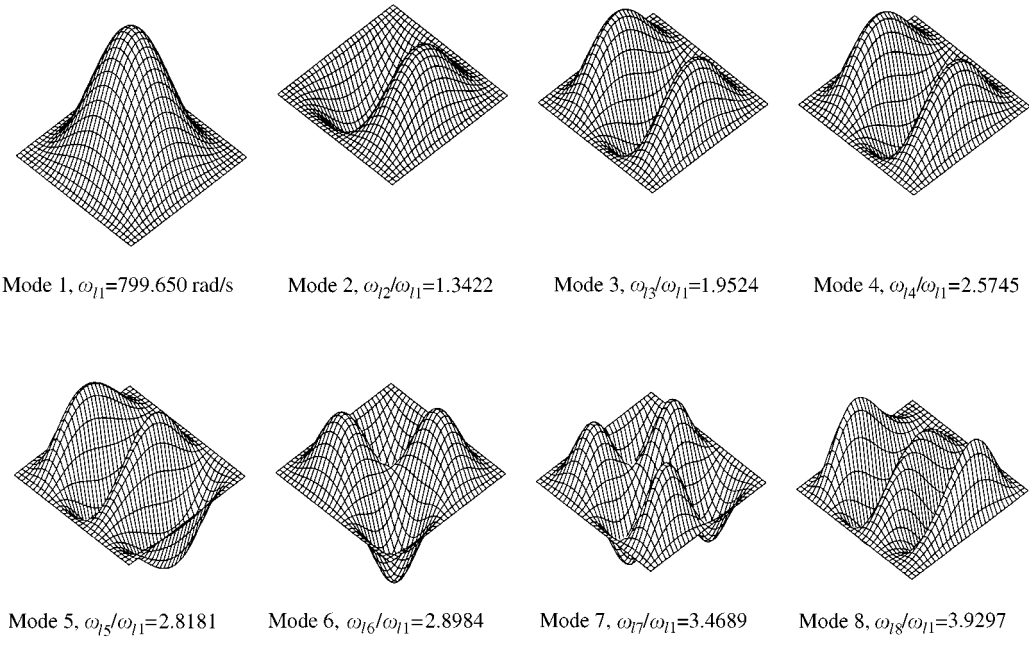

Figure 4. Linear mode shapes and natural frequencies of Plate 2, $\theta = 15^\circ$, $p_o = 8$.

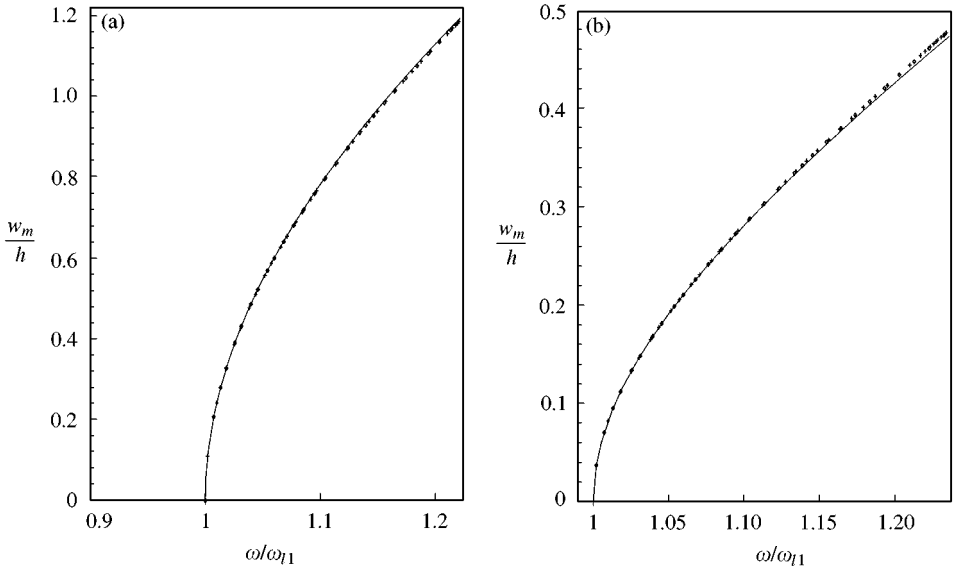

Figure 5. Total displacement calculated with: (−) one harmonic, (◇) two harmonics, (+) three harmonics. Plate 1. (a) $(\xi, \eta) = (0, 0)$. (b) $(\xi, \eta) = (0{\cdot}5, 0{\cdot}5)$.

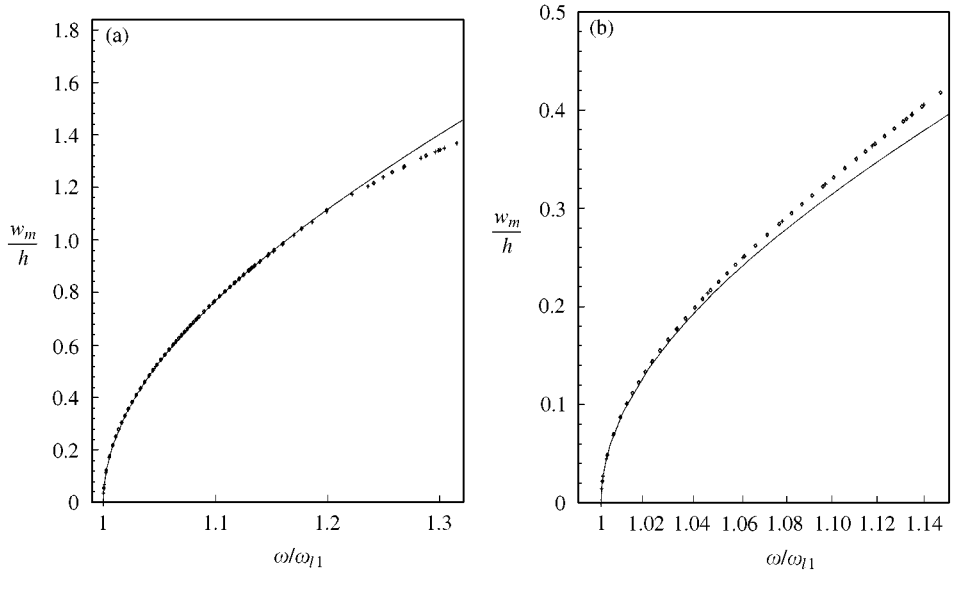

Figure 6. Total displacement calculated with: (−) one harmonic, (◇) two harmonics, (+) three harmonics. Plate 2. (a) $(\xi, \eta) = (0, 0)$. (b) $(\xi, \eta) = (0{\cdot}5, 05)$.

4.3. CONVERGENCE WITH THE NUMBER OF SHAPE FUNCTIONS

4.3.1. Out-of-plane shape functions

Table 3 shows that an HFEM model with five out-of-plane shape functions (25 d.o.f.) correctly approximates the first five natural linear frequencies of Plate 1.

Figure 7 demonstrates that the backbone curve of the first harmonic of Plate 1 is well approximated with $p_o = 5$. The third harmonic requires six out-of-plane shape functions, although five give a very reasonable approximation. W_1 and W_3 represent, respectively, the amplitudes of the first and third harmonics at the points (ξ, η) indicated in the figures and are given by

$$W_1 = \lfloor \mathbf{N}_w \rfloor \{\mathbf{w}_1\}, \tag{36}$$

$$W_3 = \lfloor \mathbf{N}_w \rfloor \{\mathbf{w}_3\}. \tag{37}$$

Table 4 demonstrates that a model constructed with five out-of-plane shape functions (25 d.o.f.) correctly approximates the first eight linear natural frequencies of Plate 2. Table 5 compares the HFEM results with results from reference [22] and

TABLE 3
Linear natural frequencies (rad/s) of Plate 1

p_o	5	6	7	10
d.o.f.	25	36	49	100
ω_1	4941·817	4941·817	4941·533	4941·484
ω_2	7302·876	7300·268	7300·230	7299·848
ω_3	10904·63	10904·63	10894·69	10894·44
ω_4	12223·93	12220·70	12219·51	12219·32
ω_5	14994·59	14979·04	14979·04	14977·37

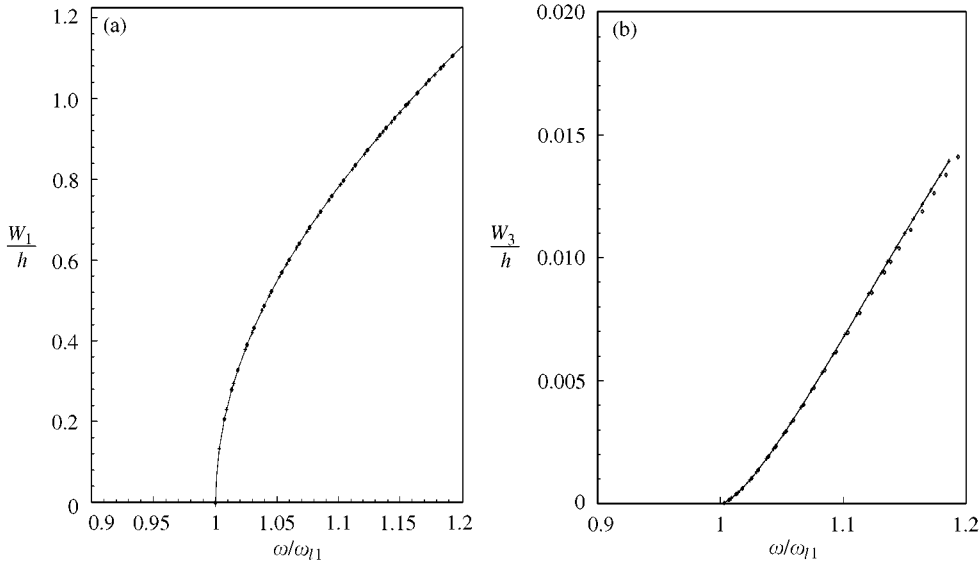

Figure 7. Plate 1. Amplitudes calculated at point $(\xi, \eta) = (0, 0)$ with $p_i = 6$ and: ($\diamond$) $p_o = 5$, ($-$) $p_o = 6$, ($+$) $p_o = 7$.

TABLE 4
Linear natural frequencies (rad/s) of Plate 2

p_o	5	6	7	8
d.o.f.	25	36	49	64
ω_1	763·159	763·101	763·097	763·096
ω_2	1420·46	1419·97	1419·93	1419·93
ω_3	1648·23	1647·45	1647·38	1647·36
ω_4	2220·85	2220·10	2219·17	2219·13
ω_5	2657·12	2654·92	2650·82	2650·65
ω_6	2872·60	2869·40	2865·34	2865·10
ω_7	3210·34	3198·62	3194·66	3193·69
ω_8	3793·95	3730·63	3721·23	3715·73

TABLE 5
Linear natural frequency parameter of Plate 2, $\theta = 45^\circ$, $\lambda = (\rho h \omega^2 a^4 / D_0)$, $D_0 = (E_L h^3)/(12(1 - \nu_{LT}\nu_{TL}))$

Mode	1	2	3	4	5	6	7	8
HFEM $p_o = 8$ 64 d.o.f.	22·38	41·65	48·32	65·09	77·74	84·03	93·67	109·0
HFEM $p_o = 6$ 36 d.o.f.	22·28	41·65	48·32	65·11	77·87	84·16	93·81	109·4
Rayleigh–Ritz [22] 50 terms	22·40	41·64	48·32	65·09	77·76	84·06	93·58	109·0

a good agreement is found. Figure 8 shows the backbone curves of the first and third harmonics of Plate 2 calculated with different numbers of out-of-plane shape functions. With $p_o = 5$ a good approximation is obtained.

4.3.2. *In-plane shape functions*

Figure 9 shows that six in-plane shape functions are enough to approximate the first harmonic of Plate 1 and that the third harmonic requires eight in-plane shape functions.

The first harmonic of Plate 2, is accurately calculated with seven in-plane shape functions and the third harmonic requires, for the frequency regions considered, eight in-plane shape functions: Figure 10. Figures 9 and 10 demonstrate that the number of in-plane shape functions necessary increases with the amplitude of vibration.

4.4. MODAL COUPLING

4.4.1. Plate 1

In this section Plate 1 is analyzed using a model with $p_o = 6$, $p_i = 10$ and two harmonics (72 d.o.f.). In Figures 11 and 12 the branch diagrams of Plate 1 are

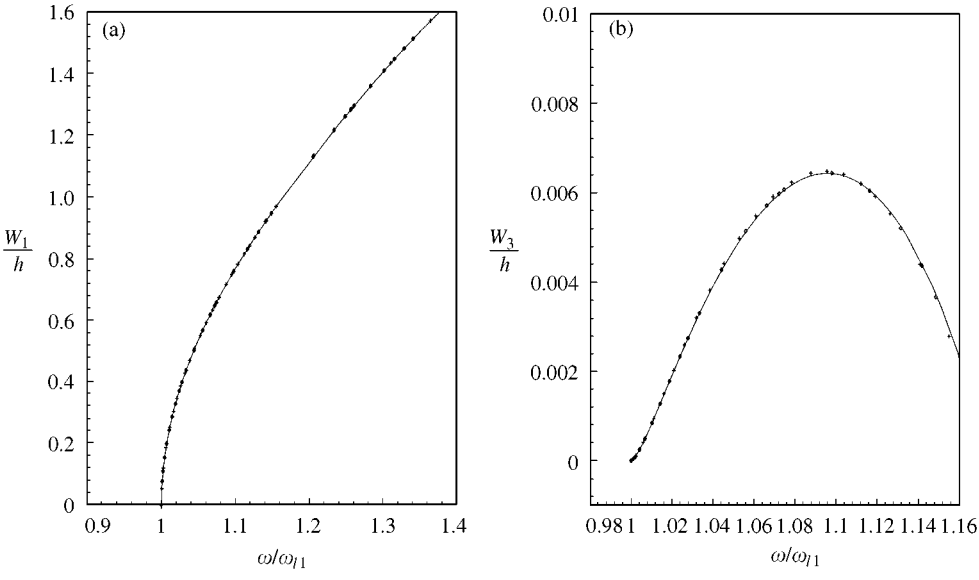

Figure 8. Plate 2. Amplitudes calculated at point $(\xi, \eta) = (0, 0)$ with $p_i = 10$ and: $(-)$ $p_o = 5$ $(\diamond)$ $p_o = 6$, $(+)$ $p_o = 7$.

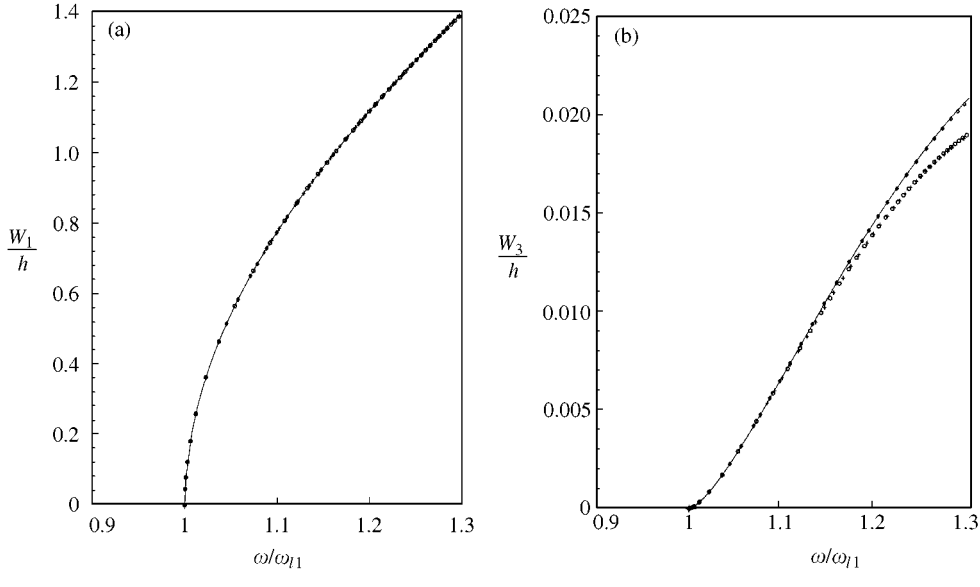

Figure 9. Plate 1. Amplitudes calculated at point $(\xi, \eta) = (0, 0)$ with $p_o = 6$ and: $(-)$ $p_i = 6$, $(\diamond)$ $p_i = 7$, $(+)$ $p_i = 8$, $(\bigcirc)$ $p_i = 10$.

shown. There are two main branches, each of them with one bifurcation point. From these points originates a secondary branch that connects the main branches.

The first main branch begins at the first linear mode and is defined mainly by the first harmonic. Figures 13(a, b) show sections of the mode shapes of the first and

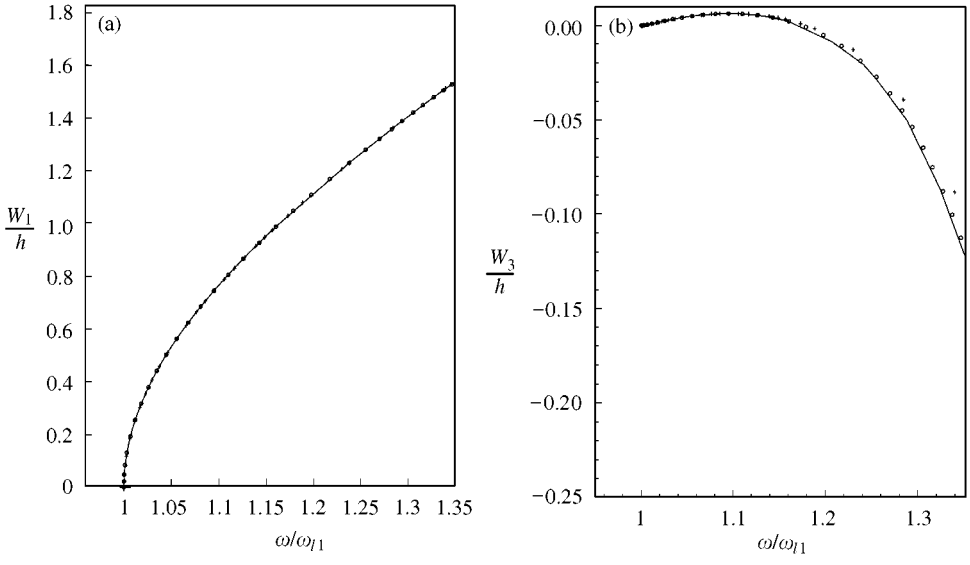

Figure 10. Plate 2. Amplitudes at point $(\xi, \eta) = (0, 0)$ calculated with $p_o = 5$ and: $(+)$ $p_i = 7$, $(\bigcirc)$ $p_i = 8$, $(-)$ $p_i = 10$.

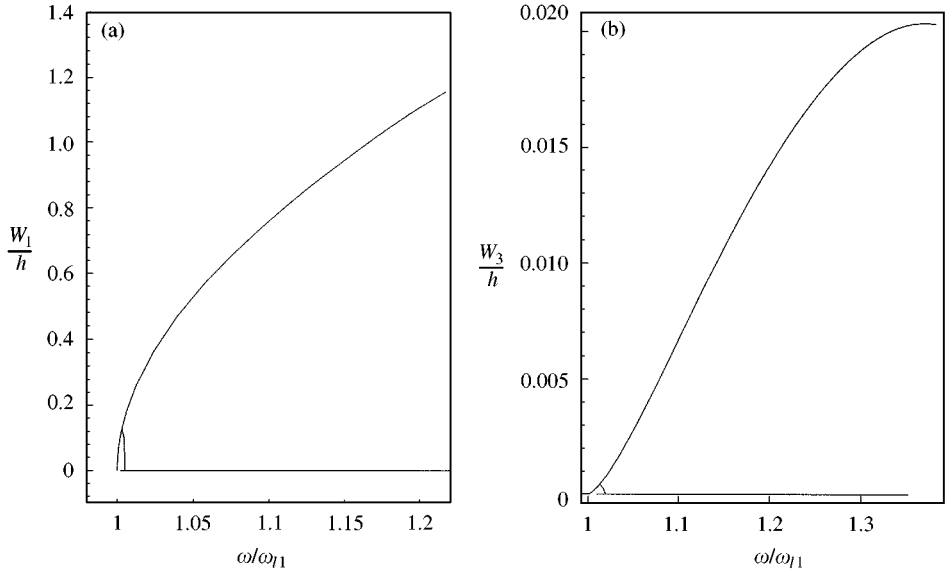

Figure 11. Branch diagrams of Plate 1. Amplitudes calculated at $(\xi, \eta) = (0, 0)$.

third harmonics in this branch. Figure 13(c) represents the normalized shape of the plate at $t = 2\pi mT$, where m is an integer and T represents the period of vibration. The first harmonic's mode shape changes with amplitude, but remains similar to the first linear mode shape. The second harmonic's mode shape changes more with the amplitude, but its effect is very small and the plate vibrates essentially in its first mode.

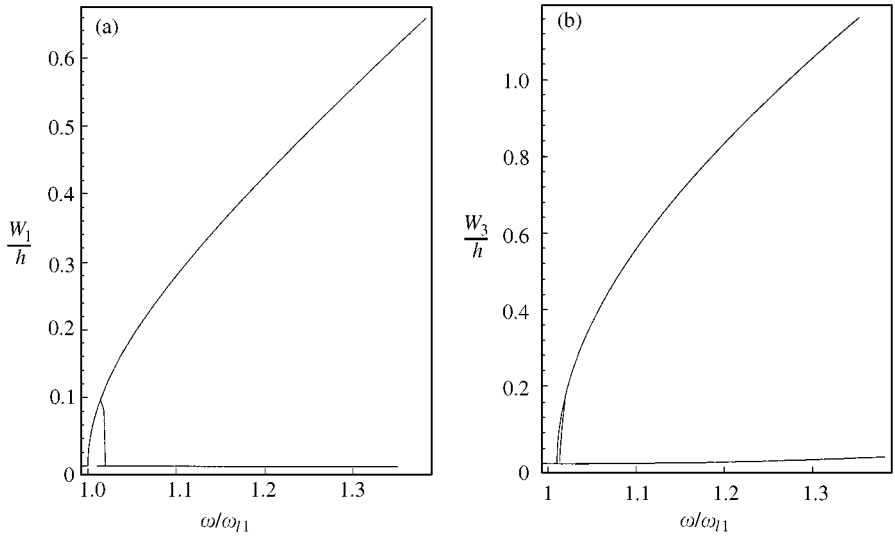

Figure 12. Branch diagrams of Plate 1. Amplitude calculated at $(\xi, \eta) = (0{\cdot}5, 0{\cdot}5)$.

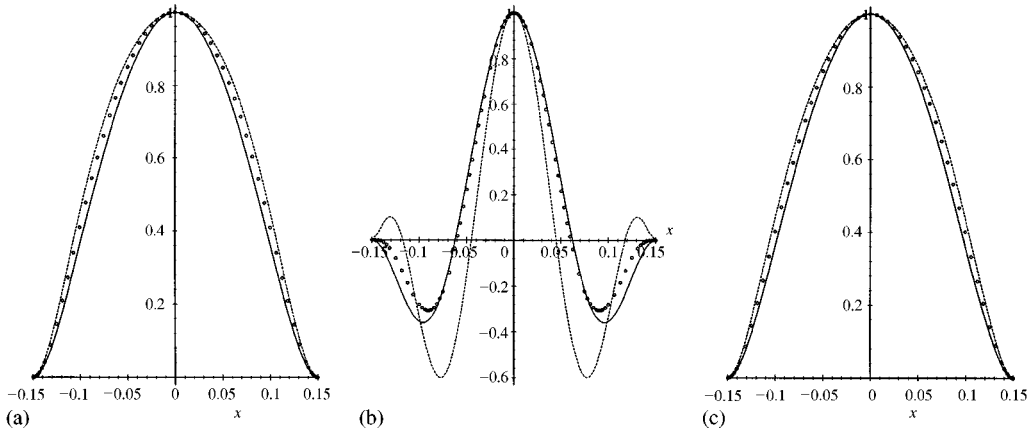

Figure 13. Sections of modes of Plate 1 at $y = 0$, first main branch at points $(-)\omega/\omega_{l1} = 1{\cdot}0004$, $(\bigcirc)\ \omega/\omega_{l1} = 1{\cdot}1883$, (---) $\omega/\omega_{l1} = 1{\cdot}3818$. (a) First harmonic. (b) Third harmonic. (c) Both harmonics.

The first and fifth linear natural frequencies are related by $\omega_{l5}/\omega_{l1} = 3{\cdot}03$. Therefore, when the first non-linear resonance frequency, ω_{nl1}, increases due to the increase of the stiffness with the amplitude, a 1 : 3 internal resonance occurs and results in a birfurcation point and in a secondary branch. This secondary branch finishes at a second bifurcation point in a second main branch. Moving along the secondary branch, from the bifurcation point of the first main branch to the bifurcation point on the second main branch, the importance of the first harmonic decreases and the importance of the second harmonic increases.

In the secondary branch, the *non-linear* modes of the first and third harmonics have the aspect shown in Figure 14, which is similar, but different, to the one of the

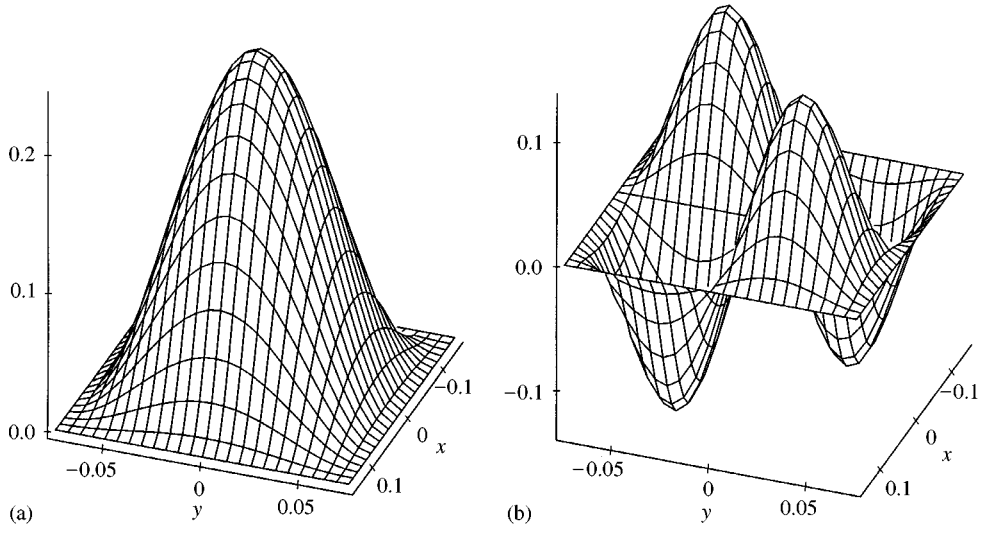

Figure 14. Mode shapes of the first (a) and third (b) harmonics, at point $\omega/\omega_{l1} = 1{\cdot}0179$ of the secondary branch. Plate 1.

first and fifth linear modes. In this branch, the plate's mode shape changes considerably during the period of vibration, because it is described by the sum of the first and fifth modes vibrating at different frequencies. An example of this variation is shown in Figure 15. The plots were made at increments of $T/24$, and are shown for half a cycle. In the other half of the cycle the plots are symmetric to the ones presented with relation to the plane x–y.

The second main branch is defined by the fifth mode of vibration and the third harmonic.

4.4.2. *Plate* 2

Plate 2 with $\theta = 45^\circ$ is analyzed by using a model with $p_o = 5$, $p_i = 6$ and two harmonics (50 d.o.f.). In this plate, the importance of the third harmonic increases significantly with the amplitude of vibration, but does not result in a secondary branch: Figure 16.

Figure 17 shows the modes of the first and third harmonics for a particular point of the backbone curve. The first harmonic, Figure 17(a), vibrates in mode 1, the third, Figure 17(b), in mode 6. The linear natural frequencies of these modes are related by $\omega_{l6}/\omega_{l1} = 3{\cdot}75$. Due to the hardening spring effect $\omega_{nl1} > \omega_{l1}$ and a 1 : 3 internal resonance occurs. Consequently, modes 1 and 6 couple and the third harmonic is increasingly excited. An example of the vibration of the plate in the time domain is shown in Figure 18, where the plots represent the plate at instants in time differing by $T/24$.

Figures 19 and 20 represent sections of the mode shapes associated with the first and third harmonics, at $y = 0$ and for different frequencies of vibration, that is at different vibration amplitudes. The mode shapes of each harmonic vary with

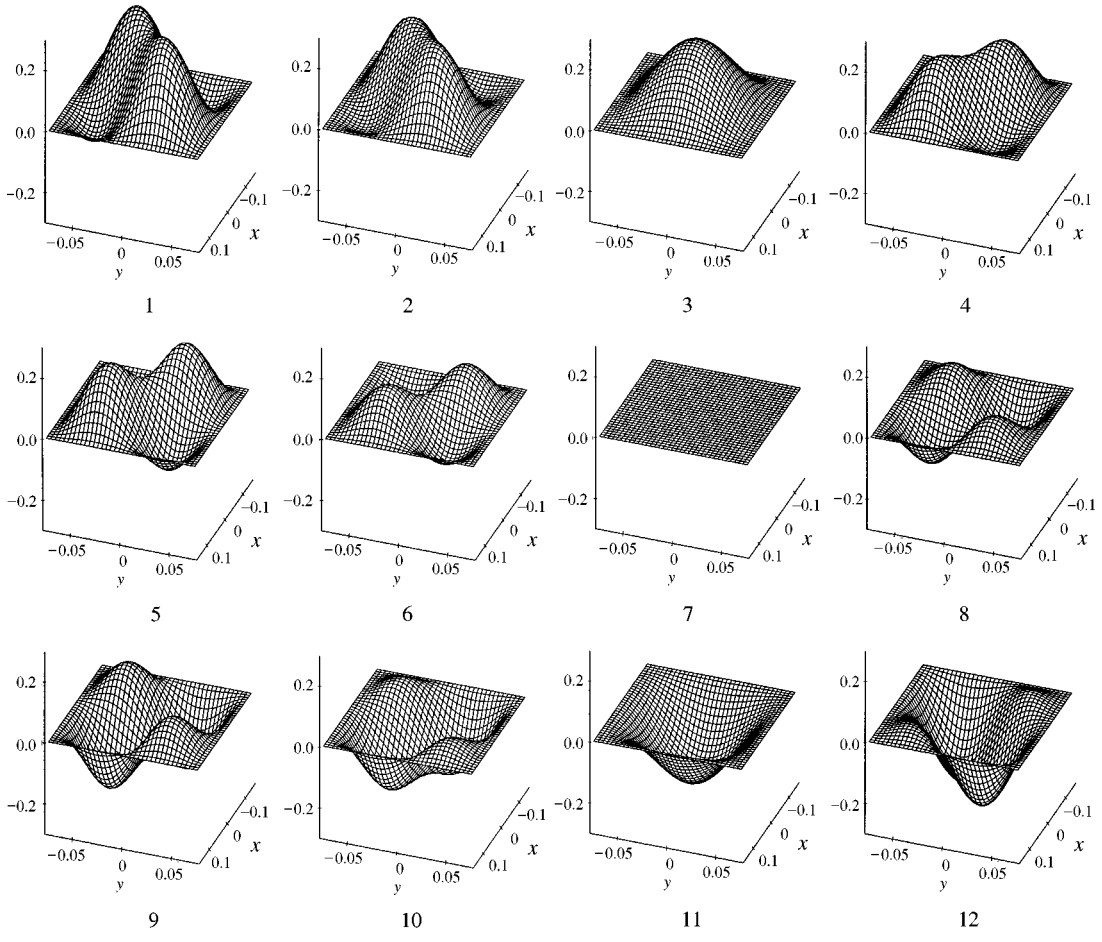

Figure 15. Vibration of Plate 1 during half a cycle, at point $\omega/\omega_{l1} = 1{\cdot}0179$ of the secondary branch.

amplitude, but remain similar to the first and sixth modes. Figure 21 shows a section of the plate, which is defined by both the first and third harmonics. The total shape of the plate varies with the amplitude because the mode shapes of each harmonic vary and, more significantly, because the relative weight of each harmonic also changes with amplitude.

Because the internal resonance is of the type 1 : 3, the two and three harmonics approximations give the same results as shown in Figure 6.

Tables 6 and 7 show that modes 1–7 of Plate 2, $\theta = 15^\circ$, are well approximated with six out-of-plane shape functions (36 d.o.f.). A model with six out-of-plane shape functions, 10 in-plane shape functions and two harmonics, i.e. 72 d.o.f. will be used in the analyses of this plate.

The first mode and first linear frequency of Plate 2 only vary slightly with the orientation of the fibres. However, higher order modes have quite different natural frequencies and mode shapes: Figures 3 and 4.

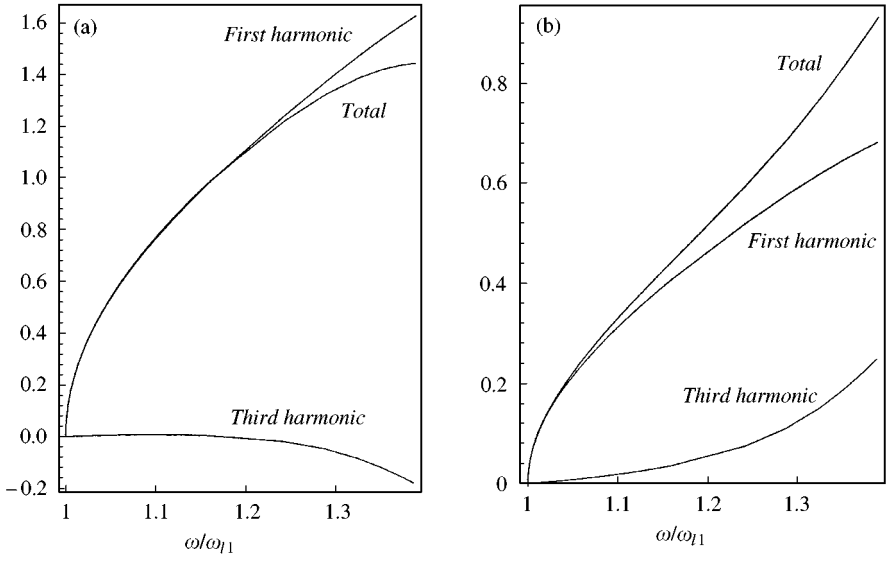

Figure 16. Backbone curves of Plate 2. (a) $(\xi, \eta) = (0, 0)$. (b) $(\eta, \xi) = (0{\cdot}5, 0{\cdot}5)$.

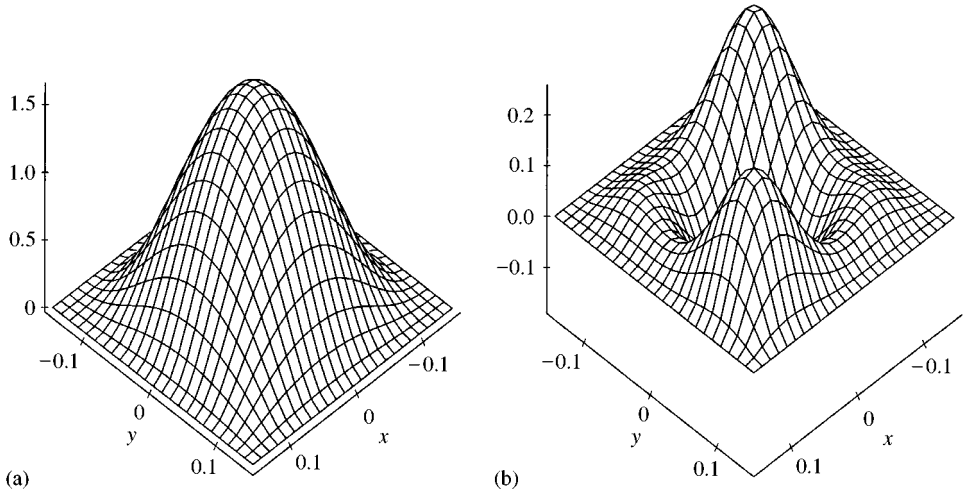

Figure 17. Mode shapes of the first (a) and third (b) harmonics, at point $\omega/\omega_{l1} = 1{\cdot}3868$. Plate 2.

Figure 22 compares the first harmonic's backbone curve of Plate 2 when $\theta = 45^\circ$ and when $\theta = 15^\circ$. The slope of the curves is different, showing that the stiffness of Plate 2 increases more with amplitude if $\theta = 15^\circ$ than if $\theta = 45^\circ$.

Whilst with $\theta = 45^\circ$ the third harmonic amplitude increases initially and afterwards decreases significantly, due to the internal resonance, and becomes negative, with $\theta = 15^\circ$ it increases slowly and uniformly, without becoming so important—Figure 23.

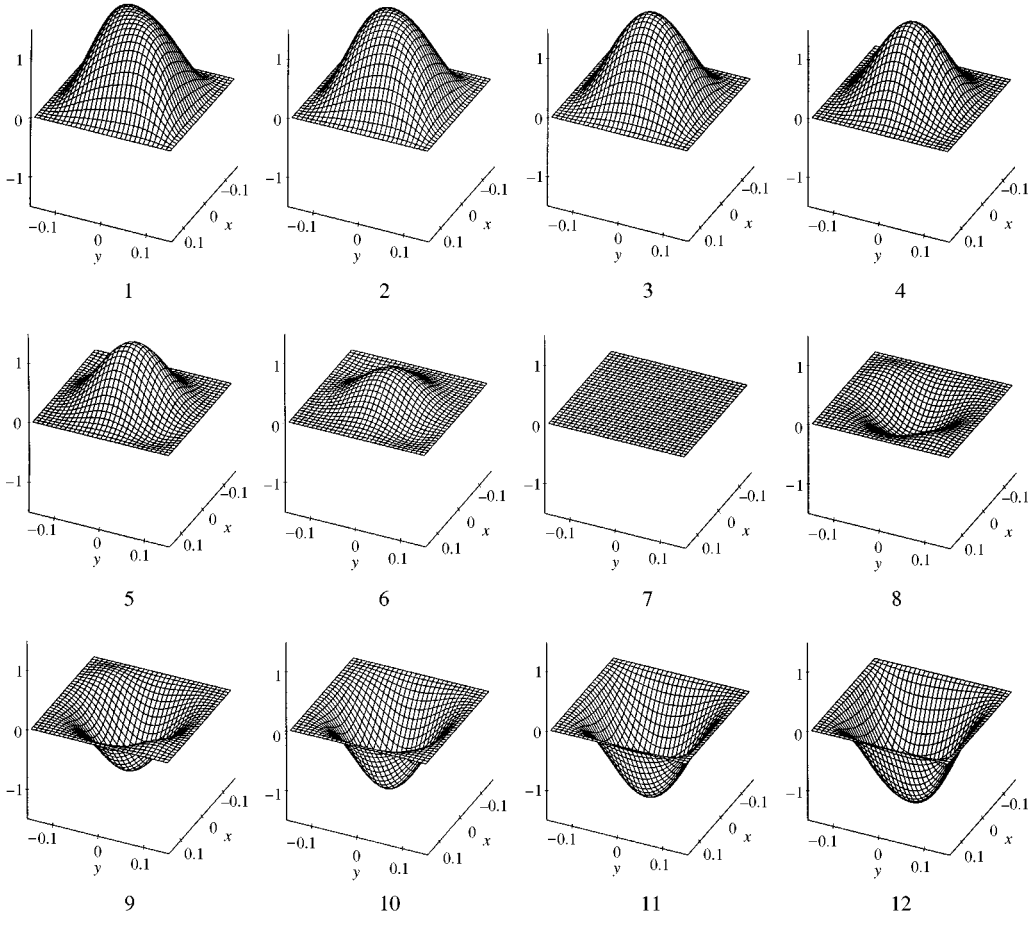

Figure 18. Vibration of Plate 2 during half a cycle, at point $\omega/\omega_{l1} = 1{\cdot}3868$.

5. CONCLUSION

The geometrically non-linear periodic free vibration of laminated composite plates was studied using the hierarchical finite-element and harmonic-balance methods.

The convergence with the number of shape functions and with the number of harmonics was analyzed and it was demonstrated that an accurate model is obtained with a reduced number of d.o.f.

Internal resonances were detected and their consequences discussed. In what concerns the backbone curve, they result either in a secondary branch or in an increase of the curvature of the main branch. Because of the modal coupling of modes vibrating at different frequencies, internal resonances also result in a very significant variation of the mode shape during the period of vibration.

Another cause of the mode shape's variation is the modification of the stiffness of the plate with the vibration amplitude. In this case, the non-linear mode shape varies smoothly and maintains a close resemblance to the linear mode shape.

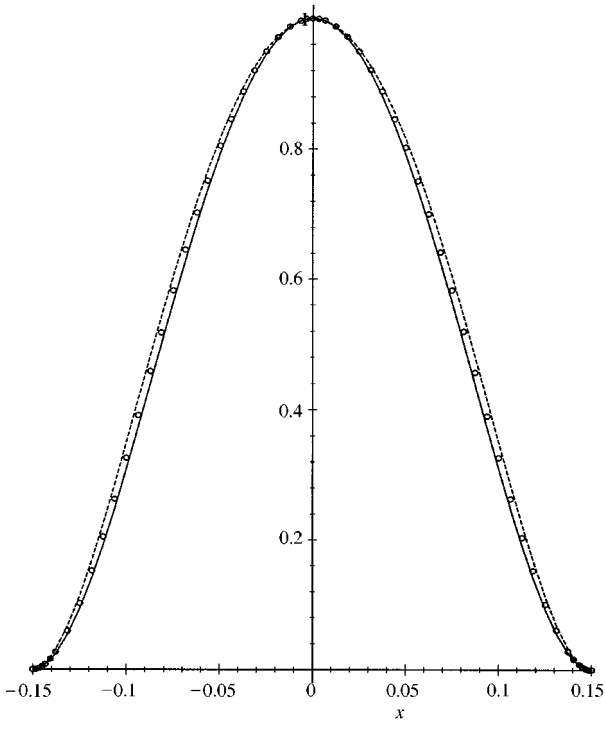

Figure 19. Sections of modes of first harmonic of Plate 2 at points (−) $\omega/\omega_{l1} = 1{\cdot}0006$, (○) $\omega/\omega_{l1} = 1{\cdot}1306$. (--) $\omega/\omega_{l1} = 1.3868$. $y = 0$.

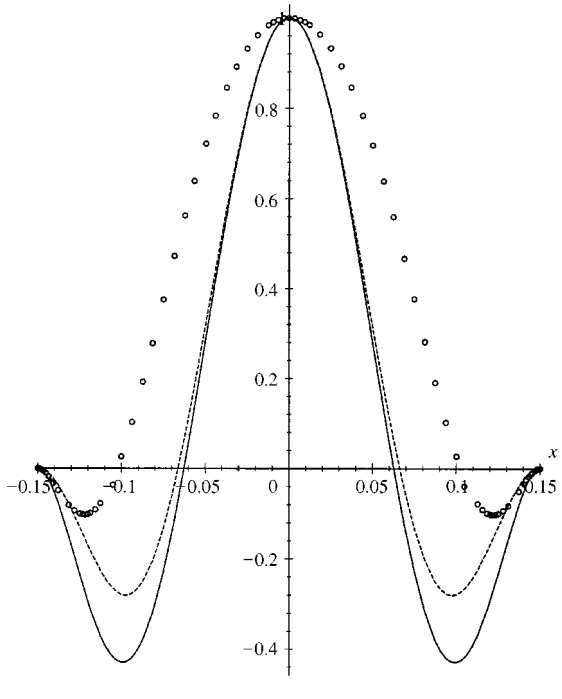

Figure 20. Sections of modes of third harmonic of Plate 2 at points (−) $\omega/\omega_{l1} = 1{\cdot}0006$, (○) $\omega/\omega_{l1} = 1{\cdot}1306$, (--) $\omega/\omega_{l1} = 1{\cdot}3868$. $y = 0$.

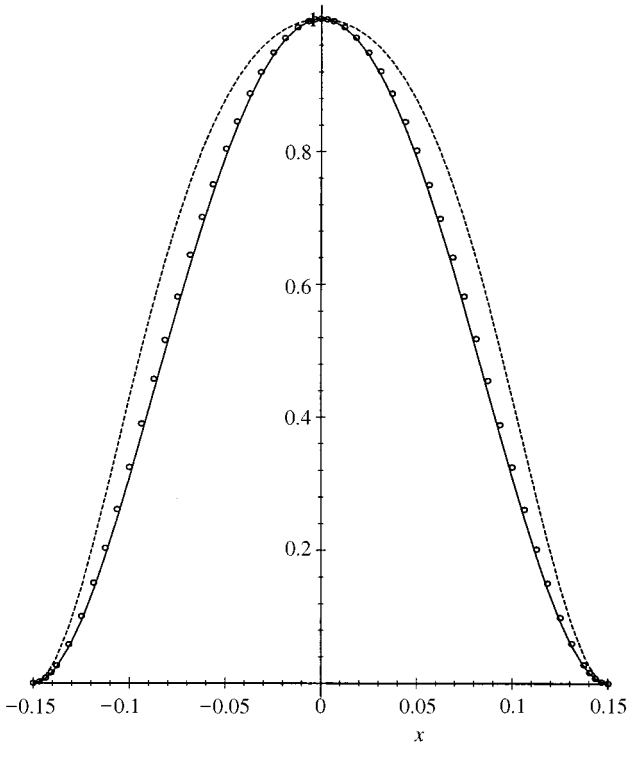

Figure 21. Sections of shape of vibration (both harmonics) of Plate 2 at $y = 0$, points (–) $\omega/\omega_{l1} = 1{\cdot}0006$, (○) $\omega/\omega_{l1} = 1{\cdot}1306$, (--) $\omega/\omega_{l1} = 1{\cdot}3868$.

TABLE 6

Convergence of linear natural frequencies (rad/s) of Plate 2, $\theta = 15$, with the number of out-of-plane shape functions

p_o	d.o.f.	ω_1	ω_2	ω_3	ω_4	ω_5	ω_6	ω_7
6	36	799·652	1073·32	1562·72	2058·84	2263·52	2318·30	2775·89
8	64	799·650	1073·30	1561·23	2058·71	2253·53	2317·71	2773·88

TABLE 7

Linear natural frequency parameter of Plate 2, $\theta = 15°$. $\lambda = (\rho h \omega^2 a^4/D_0)$, $D_0 = (E_L h^3)/(12(1 - v_{LT} v_{TL}))$

Mode	1	2	3	4	5	6	7
HFEM $p_o = 6$ 36 d.o.f.	23·45	31·48	45·83	60·38	66·39	67·99	81·41
Rayleigh–Ritz [22] 50 terms	23·46	31·48	45·86	60·38	66·47	67·96	81·36

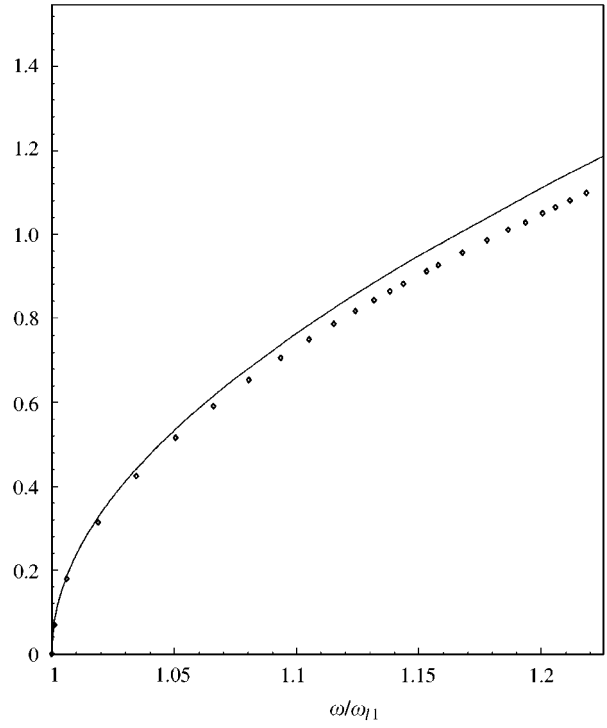

Figure 22. Amplitude of Plate 2's first harmonics: ($\diamond$) $\theta = 15°$; (——) $\theta = 45°$. $(\xi, \eta) = (0, 0)$.

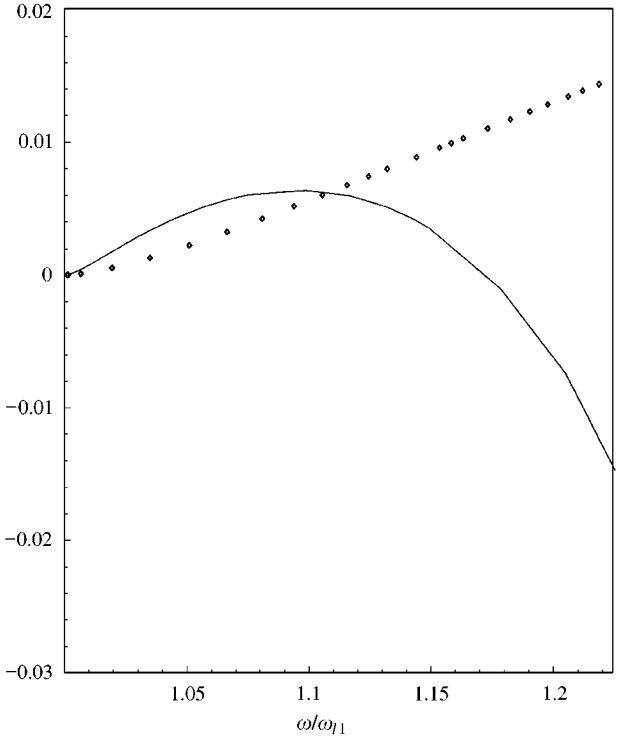

Figure 23. Amplitude of Plate 2's third harmonic: ($\diamond$) $\theta = 15°$, ($-$) $\theta = 45°$. $(\xi, \eta) = (0, 0)$.

The consequences of changing the fibres orientation of laminated plates were analyzed. The first linear mode and first linear frequency did not change much with that orientation, however, higher order linear modes changed significantly and occurred at very different frequencies. The slope of the backbone curves varies with the orientation of the fibres, because of different variation of the stiffness with amplitude and because modal coupling occurs with different modes and at different vibration amplitudes. Thus one way of avoiding internal resonance for a determined vibration amplitude, or vibration frequency, is to change the fibre orientation of the laminated plates.

ACKNOWLEDGMENTS

P. Ribeiro gratefully acknowledges the scholarship PRAXIS XXI/BD/3868/94 from the *Fundação Para a Ciência e a Tecnologia*, Portugal.

REFERENCES

1. M. M. Schwartz 1992 *Composite Materials Handbook*. New York: McGraw-Hill; second edition.
2. R. Benamar, M. M. K. Bennouna and R. G. White, R. G. 1994 *Journal of Sound and Vibration* **175**, 377–395. The effects of large vibration amplitudes on the mode shapes and natural frequencies of thin elastic structures. Part III: fully clamped rectangular isotropic plates-measurements of the mode shape amplitude dependence and the spatial distribution of harmonic distortion.
3. H. Wolfe 1995 *Ph.D. Thesis, University of Southampton*. An experimental investigation of nonlinear behaviour of beams and plates excited to high levels of dynamic response.
4. W. Han 1993 *Ph.D. Thesis, University of Southampton*. The analysis of isotropic and laminated rectangular plates including geometrical non-linearity using the p-version finite element method.
5. W. Han and M. Petyt 1997 *Computers and Structures* **63**, 295–308. Geometrically nonlinear vibration analysis of thin, rectangular plates using the hierarchical finite element method—I: The fundamental mode of isotropic plates.
6. W. Han and M. Petyt 1997 *Computers and Structures* **63**, 309–318. Geometrically nonlinear vibration analysis of thin, rectangular plates using the hierarchical finite element method—II: 1st mode of laminated plates and higher modes of isotropic and laminated plates.
7. P. Ribeiro and M. Petyt 1999 *International Journal of Mechanical Sciences* **41**, 437–459. Nonlinear vibration of plates by the hierarchical finite element and continuation methods.
8. W. Szemplinska-Stupnicka 1990 *The Behaviour of Non-linear Vibrating Systems*. Dordretch: Kluwer Academic Publishers.
9. A. H. Nayfeh and D. T. Mook 1995 *Nonlinear Oscillations*. New York: Wiley.
10. A. H. Nayfeh and B. Balachandran 1989 *Applied Mechanics Review* **42**. (Part 2), S175–S201. Modal interactions in dynamical and structural systems.
11. S. L. Lau, Y. K. Cheung and S. Y. Wu 1984 *Transactions of the ASME. Journal Applied Mechanics* **51,** 845–851. Nonlinear vibration of thin elastic plates. Part 2: Internal resonance by amplitude-incremental finite element.
12. B. Abe, Y. Kobayashi and G. Yamada 1998 *International Journal of Non-Linear Mechanics* **33,** 675–690. Two-mode response of simply supported, rectangular laminated plates.

13. R. M. Rosenberg 1966 *Advances in Applied Mechanics* **9**, 155–242. On non-linear vibrations of systems with many degrees of freedom.
14. P. Ribeiro 1998 *Ph.D. Thesis. University of Southampton.* Geometrical nonlinear vibration of beams and plates by the hierarchical finite element method.
15. R. E. Mickens 1984 *Journal of Sound and Vibration* **94**, 456–460. Comments on the method of harmonic balance.
16. M. N. Hamdan and T. D. Burton 1993 *Journal of Sound and Vibration* **166**, 255–266. On the steady state response and stability of non-linear oscillators using harmonic balance.
17. B. A. Szabó and I. Babuska 1991 *Finite Element Analysis.* New York: Wiley.
18. C. Y. Chia 1980 *Nonlinear Analysis of Plates.* New York: McGraw-Hill.
19. D. Redfern 1994 *The Maple Handbook.* New York: Springer.
20. R. Lewandowski 1994 *Journal of Sound and Vibration* **170**, 577–593. Non-linear free vibrations of beams by the finite element and continuation methods.
21. R. Seydel 1988 *From Equilibrium to Chaos. Pratical Bifurcation and Stability Analysis.* New York: Elsevier Science.
22. S. T. Chow, K. M. Liew and K. Y. Lam 1992 *Composite Structures* **20**, 213–226. Transverse vibration of symmetrically laminated rectangular composite plates.